Work on Nb_3Sn Cavities at Wuppertal

M.Peiniger*, M. Hein, N.Klein, G.Müller, H.Piel and P.Thüns

Fachbereich Physik der Bergischen Universität - Gesamthochschule Wuppertal
D-5600 Wuppertal, West Germany

1. INTRODUCTION

Because of its high critical temperature of 18.2 K and its corresponding high thermodynamical critical field of 535 mT the A15 compound Nb_3Sn is a promising material for superconducting accelerator cavities. Nb_3Sn cavities should allow higher accelerating fields than niobium resonators and the Joule losses should be reduced by more than two decades compared to the ones in niobium at a given temperature. Nb_3Sn accelerating structures in the frequency range below 6 GHz should therefore be applicable with high efficiency already at 4.2 K. The brittleness of Nb_3Sn which complicates its application to superconducting magnets is of no disadvantage on the surface of mechanically stable microwave resonators.

Most of the early experimental work was carried out at X-band frequencies between 8 and 10 GHz with Nb_3Sn cavities produced by the vapor diffusion technique [1-3]. Due to the high residual surface resistance improvement factors of only 40 to 70 were obtained at 4.2 K. Maximum surface magnetic fields of up to 890 Oe [2] were achieved. Although these values are below expectation they would be more than competitive to the niobium results if they could be obtained in low frequency accelerating cavities.

In Wuppertal investigations of Nb_3Sn cavities started at 8 GHz around 1974 [4]. In 1979 the first experimental acceleration of 80 KeV electrons was performed in a three cell Nb_3Sn coated 8 GHz structure [5,6]. In the last years, initiated by work on superconducting accelerator projects in Darmstadt and DESY, further investigations on Nb_3Sn cavities at 3 GHz [7,8,28] and 1 GHz were carried out. The work on Nb_3Sn was also extended to 22 GHz in order to study frequency dependent mechanisms [9,12] and to apply K-band pill box cavities to a single atom maser [13,31]. This report summarizes the results of experiments with Nb_3Sn cavities performed at Wuppertal during the time after the last workshop in CERN.

---

*) Now at Interatom GmbH, Accelerator and Magnet Technology Department
D-5060 Bergisch-Gladbach, W.Germany

2. THE FABRICATION OF A NB_3SN CAVITY

The fabrication of Nb_3Sn cavities at Wuppertal is performed by coating single and multicell niobium accelerating cavities by the vapor diffusion process in UHV furnaces especially designed for this purpose. Using this method the inner surface of a niobium cavity is exposed to a tin atmosphere of about 10^{-3}mbar at temperatures between 1050°C and 1250°C and covered with a Nb_3Sn layer of a few μm in thickness. During the last years this coating technique was developed further and applied at 22 GHz [9,12] and to single and multicell accelerating structures at 1 and 3 GHz [7,8] . In order to prepare the 1 GHz structures a new Nb_3Sn coating furnace had to be designed and constructed.

2.1. General experimental procedure

The production of a Nb_3Sn cavity can be divided into four steps. At first a cavity is manufactured from niobium following the standard procedures. Our 1 and 3 GHz cavities were deep drawn from 2 mm sheet material and the K-band pill box cavity was machined from bulk niobium. It is important that it is an all niobium cavity because of the high processing temperatures during the tin diffusion process. The rf surface of the cavity has to be as free of defects as possible, because defects which cause thermal instabilites at high fields will most likely not be influenced by the Nb_3Sn coating procedure and also limit the performance of the processed Nb_3Sn cavity. Before the tin processing the niobium cavities are therefore tested to insure their rf performance in the superconducting state.

As a second step the formation of nucleation centers of Nb_3Sn on the niobium surface is essential. This is done following a procedure developed at Siemens, Erlangen [10] . The niobium cavity is anodized with a layer of Nb_2O_5 (about 500Å in thickness) and mounted into the Nb_3Sn processing furnace (Fig. 1). A small tray is suspended freely from the top of the cavity into its interior and filled with a small amount (about 20 μg per cm^2 of cavity surface) of $SnCl_2$. The tin chloride evaporates at about 500°C and forms a tin layer on top of the Nb_2O_5 surface. At about 600°C the Nb_2O_5 layer disintegrates, the oxygen is absorbed by the niobium and the niobium surface is very quickly brought into contact with the deposited tin layer. It is assumed that a uniform layer of Nb-Sn-nucleation centers is formed at this time. The exact mechanism underlying the formation of nucleation centers of Nb_3Sn is unknown. The growth of such centers however appears to depend critically on the grain size of the niobium, on the density of cristallographic defects (produced for example by the deep drawing process) and on the purity of the base material. As the temperature is increased the nucleation centers have to have the possibility to grow. This is possible only if enough tin atoms are supplied from the tin source which is heated separately in our set up. There has to be a balance between the number of tin atoms per unit time diffusing into the surface (the absorption rate) and the number of atoms per unit time which are offered for this process. The

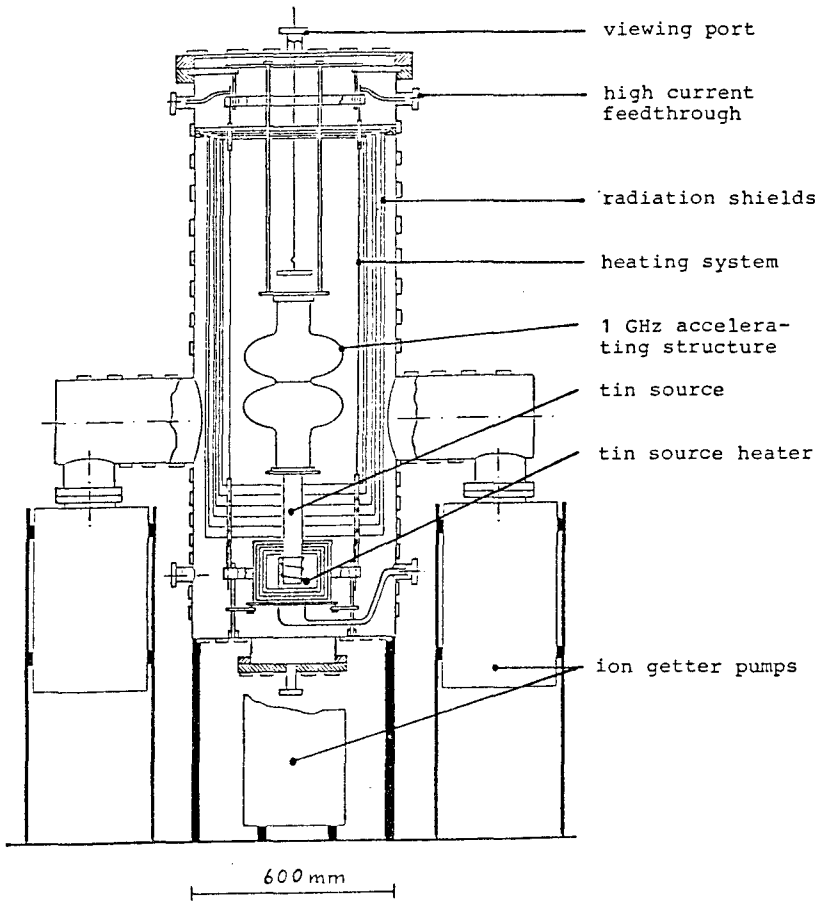

Fig. 1:

Nb_3Sn coating furnace for 1 GHz accelerator cavities

absorption rate depends on the temperature of the niobium cavity. The number of tin atoms offered for this process is directly related to the tin vapor pressure at the cavity surface. This pressure can be adjusted by the temperature of the tin source. It is at all times below 10^{-3} mbar. In considering the vapor pressure at the cavity surface one has to take into account the pressure drop between the tin source and different parts on the cavity surface caused by the finite conductance of the geometry separating the liquid tin from the cavity surface. It is apparant that the detailed balance of the nucleation process and its transition to the diffusion or layer formation process has to follow a temperature schedule for cavity and tin source which can only be determined experimentally. To find this procedure was one of the main tasks of our experimental work.

The third phase of the Nb_3Sn cavity fabrication is the formation of a Nb_3Sn layer of several μm. This process is performed at a constant temperature of the niobium cavity of typically between 1050°C and 1250 °C. The Nb_3Sn growth rate as a function of the substrate temperature, the processing time, the tin vapor pressure and the layer thickness has to be studied experimentally just like the nucleation process. The growth rate is known to depend also on the

grain size. The uniformity of the thickness of the Nb_3Sn layer over the entire rf surface of the cavity and the homogenity of its stoichiometric composition as a function of depth are two additional quantities which have to be determined by experiment for each batch of niobium characterized by a different set of material parameters. The dependence of the Nb_3Sn formation process on temperature, vapor pressure and time has been studied in some detail using small samples which were suspended inside niobium cavities during the vapor diffusion process and some typical results are described in the next paragraph.

The fourth step is the cool down of the Nb_3Sn cavity a period which so far is not well studied and during which other Nb-Sn phases can be formed which have lower critical temperatures. To remove such unwanted phases the Nb_3Sn cavity has to be subjected to a surface treatment. This is done by oxipolishing. During this process the Nb_3Sn surface of the cavity is anodized (with an anodizing voltage of typically 65 V) and the oxide layer is dissolved subsequently in hydrofluoric acid (48%). This process is repeated several times until a layer of 0.1 to 0.5 μm thickness is removed. After each of these processes the cavity is rinsed with demineralized and dust free water. After the last step it is rinsed with methanol, dyed on a dust free working bench (class 100) and mounted under the same clean condition to the vacuum system of the rf test apparatus.

2.2. Investigation of the Nb_3Sn growth kinetics on niobium samples

In order to obtain a better understanding of the empirical results obtained with Nb_3Sn cavities, we have performed several experiments with small samples (niobium sheet material of 200 μm thickness and 1 to 3 cm^2 in size) by varying the processing temperature, the processing time and the tin vapor pressure during the formation of the Nb_3Sn layer (step 3 of the fabrication process).

Two series of experiments were performed in our "small furnace" used for the coating of 3 GHz cavities (Fig. 2).

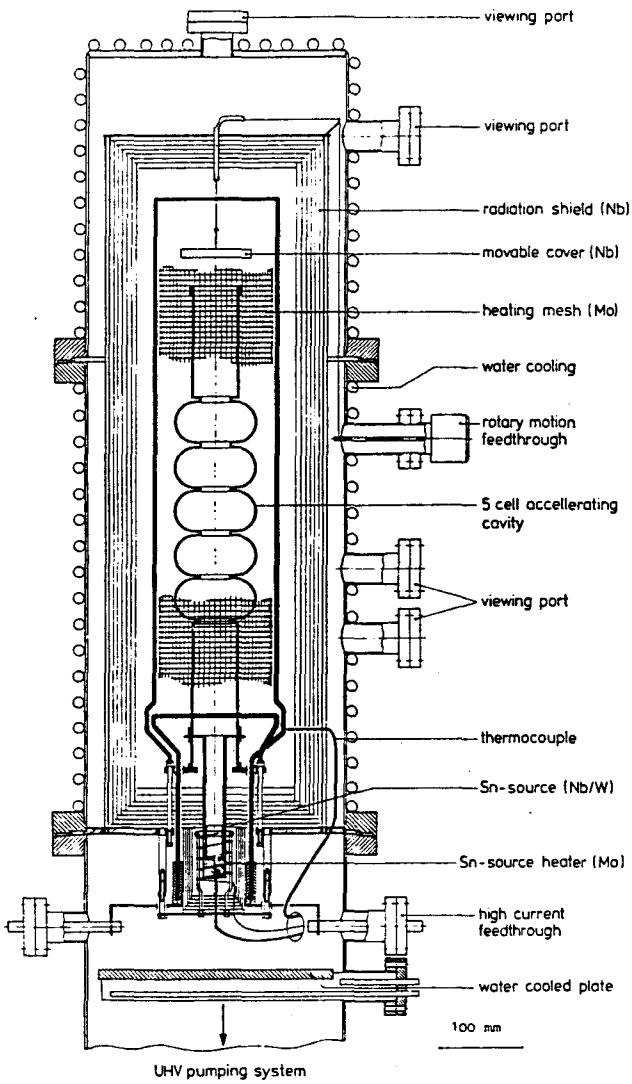

Fig. 2:
Nb_3Sn coating furnace for 3 GHz accelerating cavities.

The first set of experiments was performed on small niobium samples (1x2 cm^2 and 200 μm thick) which were suspended inside of a single cell spherical cavity by connecting them with a niobium wire to the movable cover of the cavity. The single cell cavity and the walls of the tin source, which is also fabricated of niobium, were coated during a processing time of about 40 hours with a Nb_3Sn layer of several μm to reduce the tin absorption by the chamber walls. The samples were from fine grain niobium and their residual resistivity ratio (RRR) which is a reliable measure of the purity of the niobium, was about 30 to 40. Such an RRR value is typical for all our niobium cavities which were covered with a Nb_3Sn layer. First experiments with high purity niobium (RRR > 100) will be discussed later. On fine grain niobium no special formation of nucleation centers for the Nb_3Sn coating was found to be necessary. The high density of grain bounderies appears to be sufficient for a uniform start of the Nb_3 Sn formation process.

The SEM photograph in fig. 3 shows the typical appearance of a Nb_3Sn layer of a few μm in thickness. In Fig. 4 a willfully cracked Nb_3Sn layer is shown. It indicates the columnar growth of the Nb_3Sn grains and it demonstrates that the layer thickness is roughly given by the diameter of the larger Nb_3Sn grains.

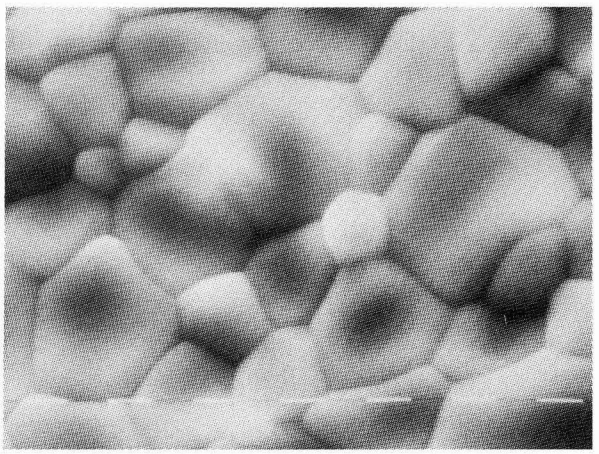

Fig. 3:
SEM photograph of a uniform Nb_3Sn layer with a thickness of about 5μm. (1 μm/div.)

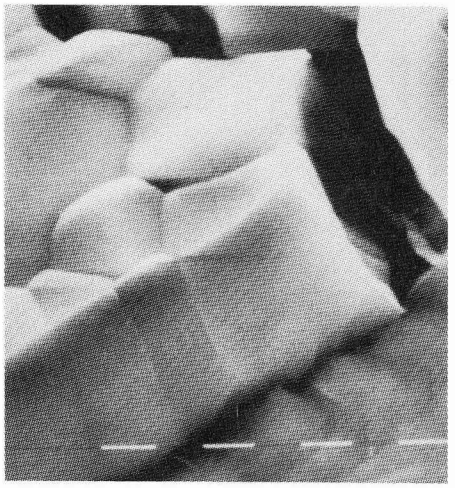

Fig. 4:
SEM photograph of a cracked Nb_3Sn layer with a thickness of about 5 μm. (1 μm/div.)

Using energy dispersive x-ray analysis the narrow electron beam of the scanning electron microscope (diameter: 0.2 μm) can be used to measure the depth profile of the stoichiometric composition of the Nb-Sn-layer on our samples [11]. Fig. 5 displays the result. The tin amount near the surface slightly exceeds that of stoichiometric Nb_3Sn but is still below the upper limit of the stable Nb_3Sn phase. An excess of tin near the surface can lead to the formation of unwanted Nb-Sn phases during the cool down of the cavity in the processing furnace.

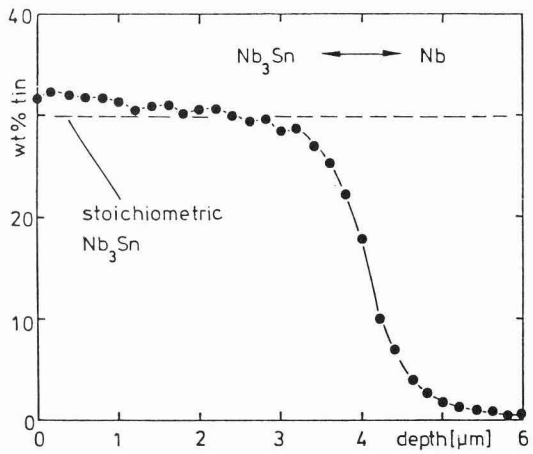

Fig. 5:
Depth profile of the Nb_3Sn layer on a niobium sample treated by the vapor diffusion technique together with a 3 GHz cavity.

It is seen that the thickness of a Nb_3Sn layer can be measured using the cracking technique (fig. 4) or by measuring the depth profile (fig. 5). A more simple procedure however was used as a standard practice. Taking into account the results displayed in figures 4 and 5 one can measure the weight increase of the sample.

From the known specific weight (8.9 gr/cm^3) of Nb_3Sn one can determine the thickness d of a Nb_3Sn layer of a few μm on a 200 μm niobium sample with a precision of a few percent.

This thickness d was measured on samples which were subjected to different processing parameters such as the processing time τ, the tin vapor pressure p_t which is determined by the temperature T_s of the tin source and the temperature T_o of the sample (or the surrounding cavity). Fig. 6 shows the thickness of the Nb_3Sn layer formed after four different processing times. The temperature of the host cavity and the sample was T_o = 1160°C and the tin vapor pressure was close to $p_t = 10^{-3}$ mbar.

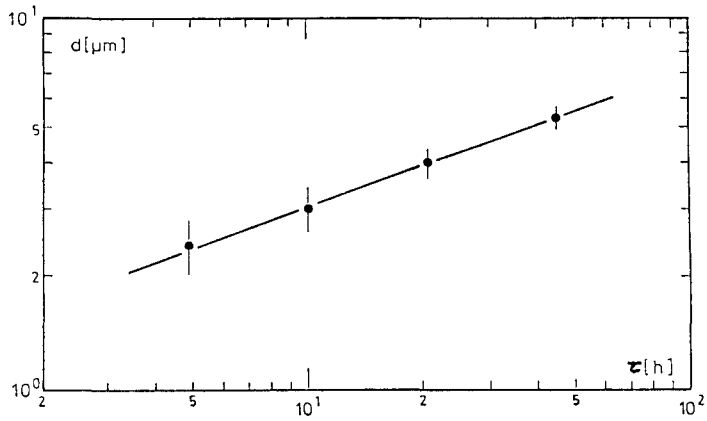

Fig. 6:
Thickness of a Nb_3Sn layer formed by the vapor diffusion technique as a function of time (reaction temperature 1160° C and tin vapor pressure about 10^{-3}Torr).

The fitted straight line in fig. 6 corresponds to a time dependence of d as given by:

$$d(\tau) = d_o \tau^{0.38 \pm 0.04} \quad (1)$$

with d_o = (1.3±0.1) μm and τ measured in hours.

The experimental value 0.38±0.04 is within errors equal to the value of 0.36 found in the literature [14–17]. The specific growth rate $d_o(T_o)$ also agrees well with data obtained by other authors, as shown in fig. 7.

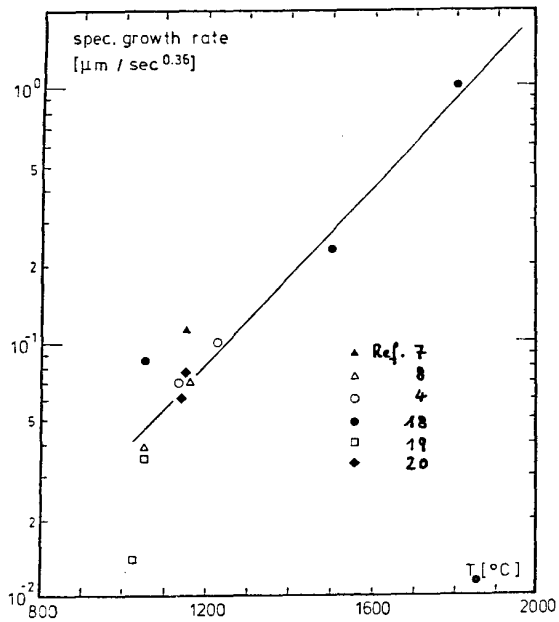

Fig. 7:
Data of the Nb_3Sn growth coefficient $d_o = d(\tau)/\tau^{0.36}$ (d_o in µm and τ in sec) as a function of niobium substrate temperature T_o

Fig. 8 shows the dependences of the layer thickness on the tin vapor pressure at a fixed processing time of 10 hours.

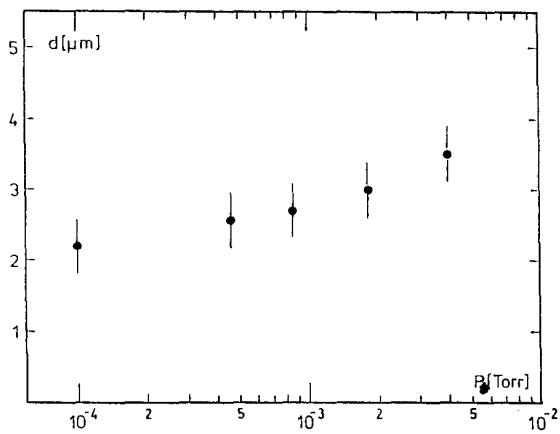

Fig. 8:
Dependence of the thickness of the Nb_3Sn layer on the tin vapor pressure.

It appears that there is only a weak dependence of d on the tin vapor pressure. This pressure however depends exponentially on the temperature T_s of the tin source and may be significantly changed by an unbalanced conductance of the geometry of tin source and cavity. The data displayed in figures 6 to 8 can therefore only be used to find an approximate set of parameters for the start of a coating experiment with a specific cavity-tin source-geometry. One or many samples suspended in a cavity to be coated are necessary to approach the correct processing parameters.

Arrangement and result of such an experiment is displayed in Fig. 9. In Fig. 9a the location of the samples during the vapor diffusion process is shown. The triangles in Fig. 9b show the layer thickness on the individual samples after a

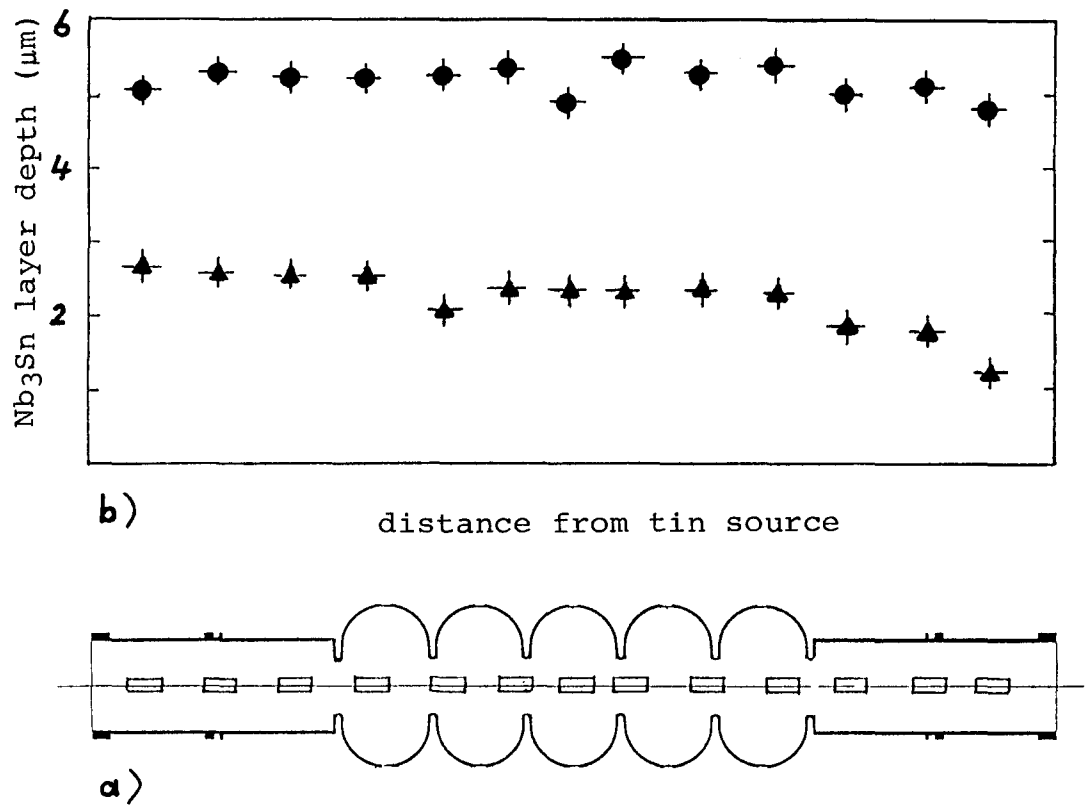

Fig. 9:
Nb_3Sn layer thickness of samples coated together with a five cell 3 GHz cavity as a function of distance to the tin source after an evaporation time of 15 hours (triangles) and after a further reaction time of 45 hours in upside down position in respect to the tin source (circles). Details are given in the text.

processing time of 15 hours. The origin for the decreasing thickness of the layer as the distance from the tin source increases is the decreasing tin vapor pressure due to the diffusion of tin into the cavity surface. In a second cycle the 5 cell cavity was therefore placed upside down on the tin source and processed again for 45 hours. The prolonged time is necessary, because the growth rate for the Nb_3Sn layer reduces in time as can be seen from eq. (1). Although the use of samples is extremely helpful to approach the correct processing parameters the final proof of a successful coating can only be found during the rf test of a superconducting Nb_3Sn cavity.,

2.3. Nb_3Sn layers on high purity niobium

The achievable accelerating fields in niobium cavities, which today are of general use in particle accelerators are limited by electron field emission and by defect induced thermal instabilities. To overcome the field limitations caused by microscopic, normal conducting defects the purity of niobium sheet material used

for the cavity fabrication has been improved significantly [21]. This was done mainly by reducing the interstitial oxygen impurities. This oxygen reduction improved the thermal conductivity of technical niobium remarkably and the obtained accelerating fields increased accordingly [22]. The residual resistivity ratio RRR of niobium is a good measure of its purity and directly proportional to its thermal conductivity λ at 4.2 K.
This relation is given by [21]

$$RRR = 4.0 \cdot \lambda(4.2\ K);\ \lambda \text{ in } W/(mK) \qquad (2)$$

For the thermal stability of normal conducting microscopic defects on a Nb_3Sn layer the thermal conductivity of the substrate niobium is as essential as in a niobium cavity. It is therefore necessary to study the formation of a Nb_3Sn layer on high purity niobium. All our previous work was done on niobium material with a residual resistivity ratio of less than 40. A first and exploratory Nb_3Sn coating experiment was carried out on a 3 GHz single cell spherical cavity fabricated from niobium of RRR = 120. Two observations were made:

- The density of Nb_3Sn nucleation centers, necessary to generate a uniform Nb_3Sn layer is stronly reduced if one uses the same processing parameters as with low RRR niobium.

- During a standard coating procedure the thermal conductivity of the niobium is lowered significantly. The reduction depends on processing time and temperature.

The physics phenomena leading to the difficulties in creating uniformly distributed Nb_3Sn nucleation centers on high purity niobium are under study but as yet not understood. Empirically it was found that uniform Nb_3Sn layers can be formed on high purity niobium if the tin vapor pressure is increased. A substrate temperature of 1100° C and a tin source temperature of 1220°C produced uniform Nb_3Sn surfaces on RRR= 200 niobium samples in a specific experiment described below. The quality of the Nb_3Sn surface appeared to be not strongly dependent of the fact if the samples were anodized or not prior to the coating procedure. The reduction of the thermal conductivity as shown in fig. 10 could be traced to the diffusion of oxygen into the high purity niobium during the tin processing. An experiment was carried out in which four RRR = 200 niobium samples were treated together with the Nb_3Sn coating of a 3 GHz single cell cavity (experimental set up in fig. 2). Two of the samples were anodized by the standard procedure (65 V anodization voltage corresponding to 1000 Å of Nb_2O_5). One pair of an anodized and not anodized sample was positioned inside the cavity (and therefore experienced the tin vapor) and the other pair was located outside of the cavity and was therefore not in contact to the tin vapor. The samples were at the same temperature as the cavity (1100°C). A high tin vapor pressure was generated by a temperature of 1220°C at the tin source. Before and after the Nb_3Sn processing the thermal conductivity of all samples was

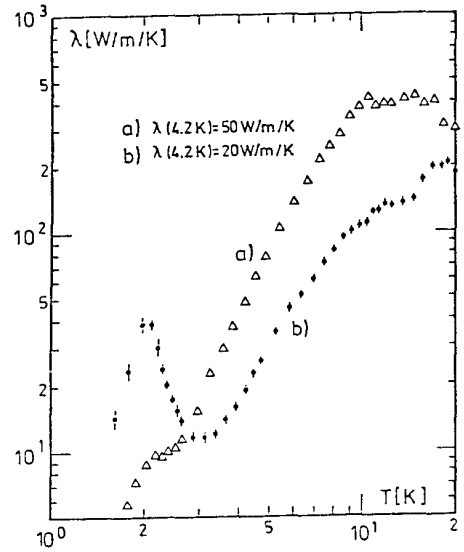

Fig. 10:
Thermal conductivity of a niobium sample as a function of temperature before (a) and after (b) the Nb_3Sn coating process. The sample was anodized with 65 V.

measured. The thermal conductivity of all samples reduced. This reduction was found to be the same for the "inside" and the "outside" samples. The tin vapor diffusion process can therefore not be held responsible. This positive result was expected as the tin diffusion process affects only a very thin surface layer which in fact turns into the wanted Nb_3Sn (see fig.5). It does not change the thermal conductivity of the bulk of the niobium substrate.

Responsible for the reduction of the thermal conductivity is the diffusion of oxygen into the high purity niobium. The RRR value of the not anodized samples reduces from 200 to 122±7 due to the high (but unknown) partial pressure of oxygen in the hot zone of the Nb_3Sn processing furnace. The anodized samples deteriorate even more due to the additional absorption of the oxygen originating from the desintegration of the Nb_2O_5 layer. There RRR falls from 200 to 77±3.

As indicated above anodizing seems not to be mandatory to obtain good Nb_3Sn surfaces if the tin vapor pressure is only kept high enough. One therefore may only have to struggle with the improvement of the oxygen partial pressure. A successful Nb_3Sn coating of rf cavities fabricated from high purity niobium may therefore be possible in the future.

3. RF EXPERIMENTS WITH SUPERCONDUCTING NB_3SN CAVITIES

3.1. The experimental programme

The rf properties of Nb_3Sn cavities were investigated on single cell cavities designed for fundamental mode frequencies of 1, 3 and 22 GHz and on a 5 cell cavity at 3 GHz in the temperature range from 2 to 20 K. In the 1 GHz cavity nine higher order modes could be excited with Q values in excess of 10^9 and

additional data at 1.8, 3 and 3.4 GHz were obtained. The temperature dependence of the rf surface resistance R_S was determined at all frequencies to find the frequency and temperature dependence as well as the absolute magnitude of the true surface resistance R_S^{BCS} of the superconducting Nb_3Sn. The temperature independent part of the surface resistance, the residual resistance R_{res}, was studied in some detail. Its dependence on thermoelectrically generated frozen in flux excited during the cool down of a Nb_3Sn cavity or during field quenching events triggered by thermal instabilities was studied at 1 and 3 GHz.

When a cavity is cooled in an external magnetic field, flux is trapped which leads to normal conducting surface areas. The residual resistance produced by their phenomenon was studied at 3 GHz and 22 GHz as a function of ambient fields in the range from 0.2 to 70 Oe.

Last but not least the field dependence of the residual losses was measured during each experiment with a superconducting Nb_3Sn cavity to gain more insight into mechanisms which lead to increasing Joule losses with increasing electromagnetic cavity fields and which finally lead to thermal instabilities.

3.2. Experimental arrangements and procedures

The Nb_3Sn cavities are fabricated as described in paragraph 2.1. The furnaces shown in figures 1 and 2 are used to coat the 1 and 3 GHz resonators. Fig. 11 shows the very similar arrangement for the processing of the K -band cavities.

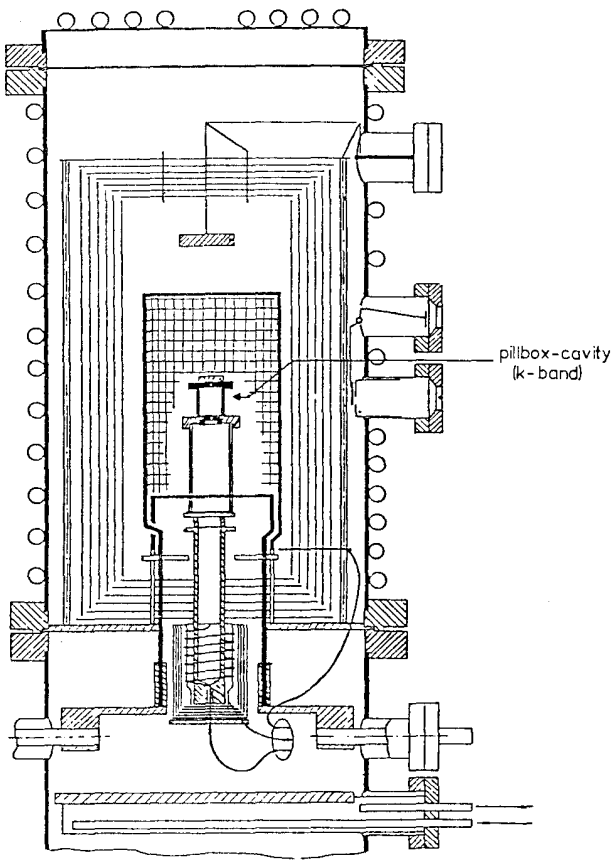

Fig. 11:
Modification of the Nb_3Sn furnace shown in Fig. 2 to process K-band cavities.

The rf tests were carried out using standard microwave techniques. In figures 12 to 14 the three cavities of 1, 3 and 22 GHz are shown schematically with their microwave couplers and vacuum lines as they are mounted inside their vertical test cryostats.

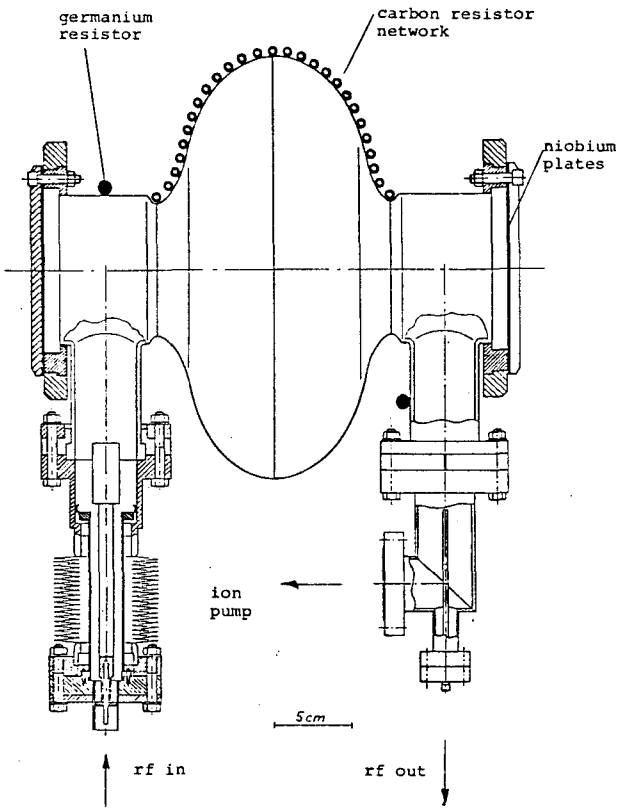

Fig. 12:
1 GHz cavity with microwave couplers and vacuum connection as it is mounted in its cryostat

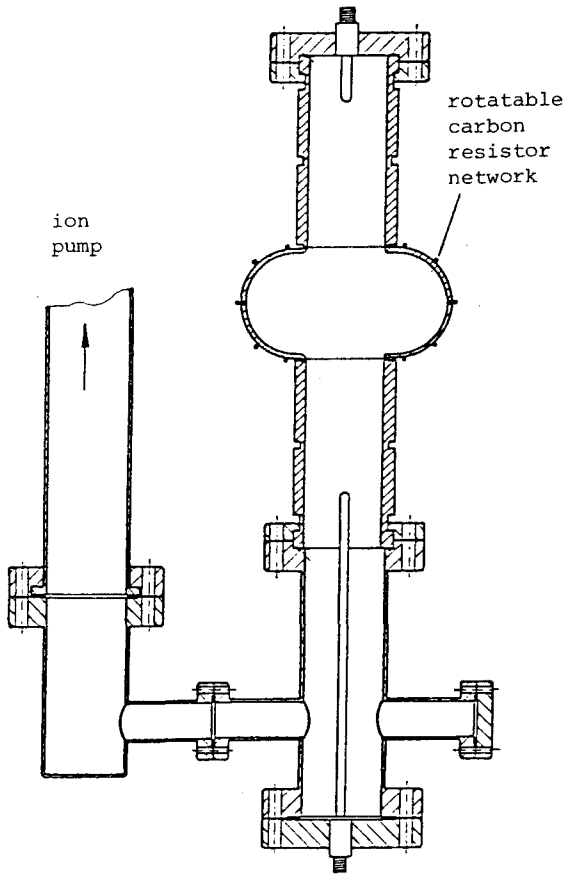

Fig. 13:
Set up of the 3 GHz cavity in its test cryostat. The magnetic shielding is not shown. The mounting of the 5 cell 3 GHz cavity is analog.

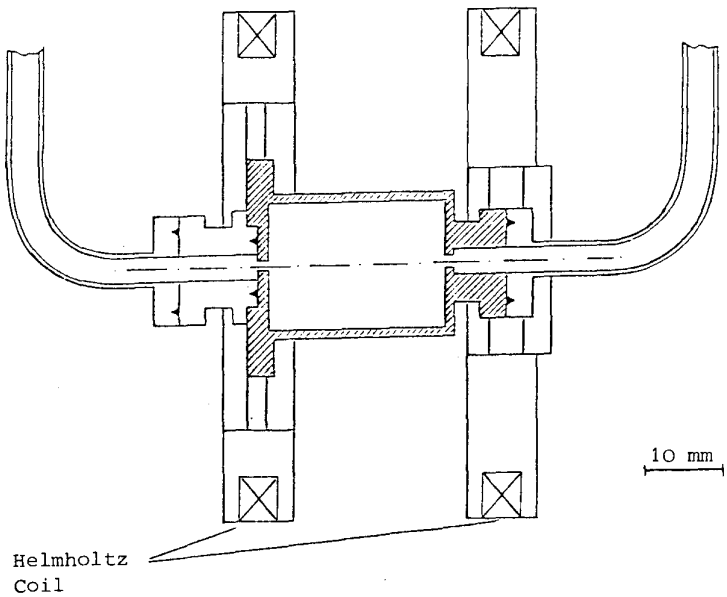

Fig. 14
K-band pill box cavity arrangement inside a vertical test cryostat. The cavity vacuum is maintained through the rectangular waveguides

At 1 and 3 GHz the microwave power is coupled to the cavities via coaxial transmission lines. At 22 GHz rectangular waveguides have to be used which at the same time act as vacuum lines. The 1 GHz cavity is equipped with a coaxial coupler, the inner conductor of which can be moved by an appropriate mechanical device from the outside of the cryostat [23] . During the measurement of the temperature dependence of R_s and the investigations of the higher order modes the problems arising from the strong Q changes or the variations in the coupling field configurations can be overcome by this variable coupler. The resonant frequencies and field distributions of the higher order modes were calculated using the computer codes SUPERFISH, URMEL and URMELT. Nearly all computed modes (about 80 between 1 and 4 GHz) could be detected using these couplers. Ten of them with frequencies between 1 and 3.4 GHz were found to show Q values higher than 10^9. They were unambigously identified by comparing the experimentally found frequencies, geometry factors and field distributions with the calculated values. To measure the cavity Q and the excited field the microwave power transmitted to the cavity is measured as well as the power reflected at the input coupler. In addition the microwave signal radiated by the output coupler is detected. The microwave power offered to the cavity can be switched by a pin modulator. From the decay time of the energy stored in the cavity after switching off the drive power, the "loaded Q" is determined. For very low Q values ($Q < 10^7$) a syntesized sweep oscillator is used to measure the frequency response of the excited field amplitude. The loaded Q is then determined from the full width at half maximum. The amplitudes of the microwave signals transmitted to and reflected from the cavity and the amplitude of the signal radiated through the output coupler are used to compute the coupling factors of the microwave couplers and the power absorbed by the cavity. Using these quantities the unloaded Q of the cavity

characterized by Q_o is determined as well as the electric and magnetic fields excited in the cavity. The quantities determined are

the unloaded Q :	Q_o
the maximum electric surface field:	E_p
the maximum magnetic surface field:	H_p
and wherever applicable	
the average accelerating field:	E_a

E_a is defined here as the energy gain experienced by the particle in traversing the cavity divided by its charge and the geometric length of its path inside the cavity. The influence of cutoff tubes at exit and entrance of the cavity is neglected.

The magnetic shielding is not shown in figure 12 to 14 but is obtained by μ-metal foils wrapped around the outside of the cryostat and in some cases also around the cavity. In any case the ambient magnetic field was reduced to values below 30 m Oe for high Q measurements.

The influence of frozen in magnetic flux on R_s generated during the cool down of the cavities was studied at 3 and 22 GHz by applying an external magnetic field. At 3 GHz this was generated by a current loop and at 22 GHz by a Helmholtz pair.

As indicated schematically in figs. 12 to 14 the cavities were mounted in vertical cryostats and immersed in liquid helium for measurements in the temperature range between 1.4 and 4.2 K. Temperatures above 4.2 K were obtained with the level of the liquid helium well below the cavity. The cavity was then cooled by the evaporating cold helium gas the mass flow of which was regulated by a heating resistor in the liquid. Germanium resistors (like indicated in fig. 13) were used to measure possible temperature gradients which can develop across the cavity. Appropriately positioned heating resistors in thermal contact to the cavity were utilized to minimize such temperature gradients between extreme locations down to tolerable values less than 1 K. This technique was used to measure the temperature dependence of R_s.

The spatial distribution of the Joule losses over the rf surface of the cavity can be measured by using the technique of temperature mapping in subcooled helium at temperatures around 2.3 K [29,25]. For this purpose a rotatable chain of Allen Bradley carbon resistors is brought into sliding contact with the outer wall of the cavity. It is used to measure the temperature signals on the outer cavity surface produced by the Joule losses on the rf sides.

4. The experimental determination of the surface resistance of superconducting Nb_3Sn

The surface resistance R_S was experimentally determined from the Q_O measurements on the different cavities and computed using the appropriate geometry factors G and the well known relation $R_S = G/Q_O$. Figure 15 shows experimental results obtained at 1, 3, 8 and 20 GHz at very low field levels. The 8GHz results are included for completeness from an earlier experiment [26]. Especially from the 1 and 8 GHz [26] data one can see that the temperature dependence of R_S can be divided into three regions. Above its critical temperature of 18 ± 0.2 K Nb_3Sn is normal conducting and shows (slightly above T_C) a surface resistance of (6.2 ± 0.3) $10^{-2}\Omega$ at 8 GHz and (1.7 ± 0.2) $10^{-2}\Omega$ at 1 GHz. Below T_C the surface resistance drops extremely steep by about four orders of magnitude within 4 K. Below 14 K the surface resistance falls exponentially and is described well for temperatures below $T_C/2$ by the relation

$$R_S(T) = A\frac{f^2}{T} e^{-\frac{\Delta}{kT}} + R_{res} \qquad (3)$$

A = Amplitude factor
f = Resonant frequency

The quantity 2Δ is the energy gap and can be interpreted as the binding energy of a Cooper pair. It is given in the BCS theory as

$$2\Delta = 2\alpha\, kT_C \qquad (4)$$

with $\alpha = 1.762$

The residual resistance R_{res} which is generated by a variety of mechanisms is assumed to be independent of temperature. This assumption is supported by the experimental data. In Fig. 15 a strong reductions of the surface resistance are observed at the critical temperature of niobium at 9.2 K and around 3.3 K where indium gets superconducting. In the case of the 1 GHz cavity the niobium flange and the indium seal at the end of the very short cutoff tubes were found responsible for these in general unusual observations. After subtracting R_{res} from R_S one obtains the true or BCS surface resistance R_S^{BCS} of the superconducting Nb_3Sn. By fitting the relation (3) to the data the frequency dependence of R_S^{BCS} at 4.2 K is obtained as well as the reduced energy gap α. Fig. 16 displays R_S^{BCS} at 4.2 K and the residual resistance of Nb_3Sn in the frequency range from 1 to 21.5 GHz. The BCS resistance for all the data between 1 and 21.5GHz is fitted very well by an f^2 dependence which is expected from the two fluid model. Calculations of R_S^{BCS} based on the BCS theory agree with the experimental value at 3 GHz if one assumes a Δ/kT_C of 2.25 a T_C of

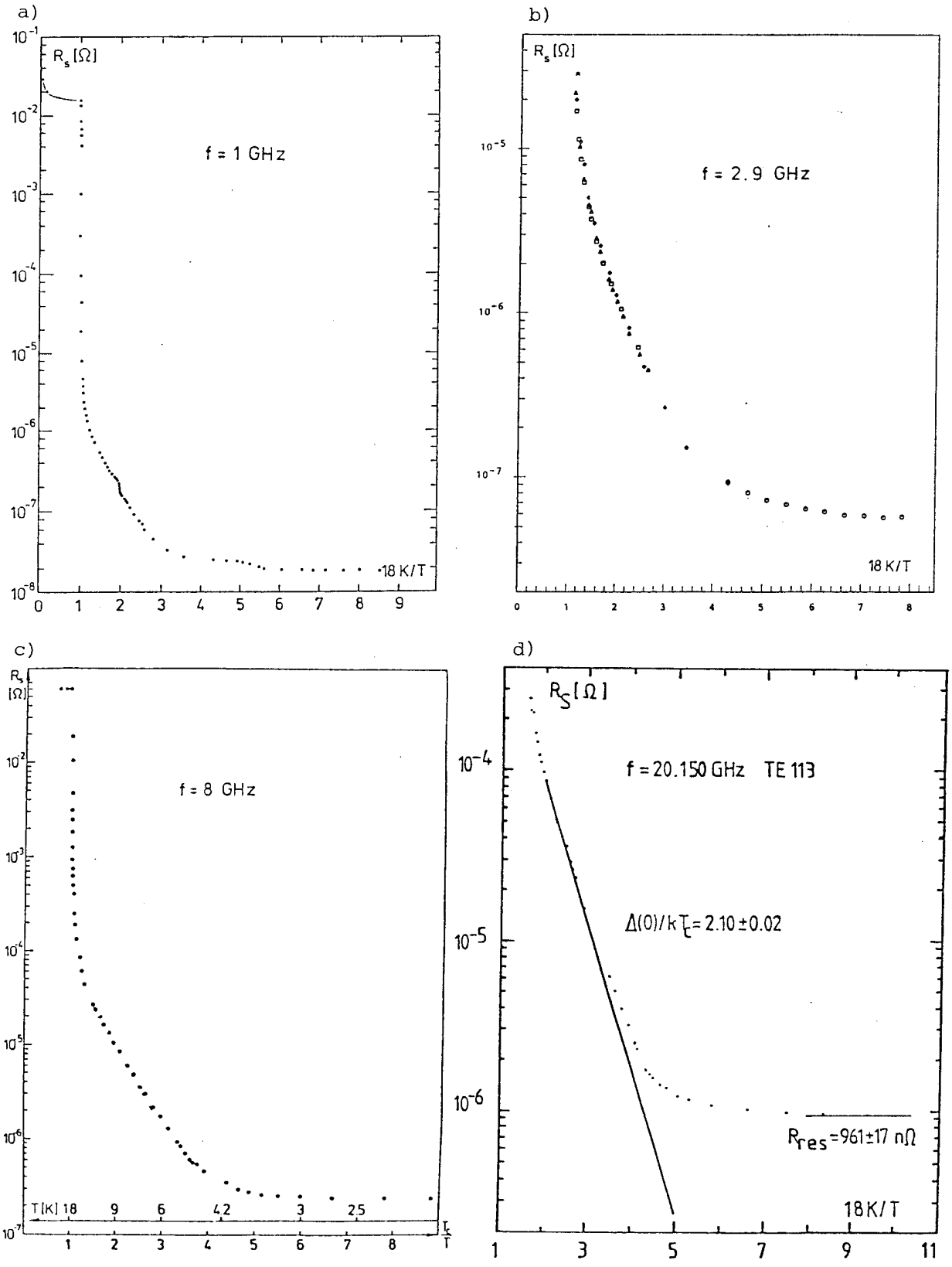

Fig. 15:
Surface resistance of Nb_3Sn as a function of temperature, measured in different cavities at 1 GHz (curve a), 2.9 GHz (curve b[7]), 8 GHz (curve c[26]) and at 20.15 GHz (curve d [7]).

SRF87E04

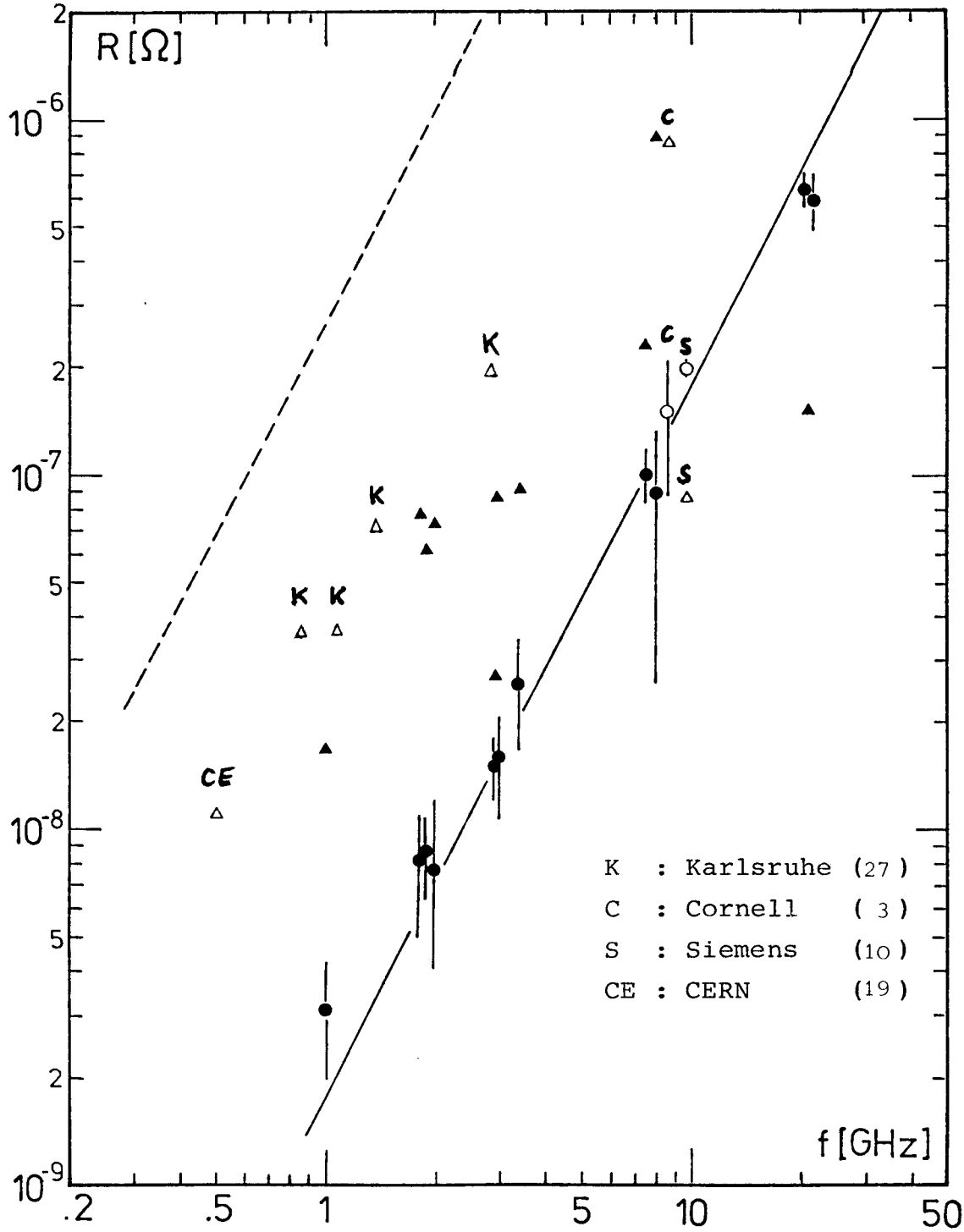

Fig. 16:
The surface resistance of superconducting Nb_3Sn at 4.2 K. The BCS-resistance (circles with error bars) measured at Wuppertal (full symbols) follows an f^2-dependence (solid line). The triangles give the residual resistance R_{res}. The dashed line shows the BCS resistance of niobium at 4.2 K.

18 K, a coherence length of 6 nm, a London penetration depth of 60 nm and an electron mean free path of 1 nm [27].

In considering only the BCS resistance of Nb_3Sn one can deduce from Fig. 16 an improvement factor of about 150 compared to the surface resistance of niobium at 4.2 K and for frequencies below 10 GHz. This picture is changed if the residual losses are taken into account, although a significant improvement remains. Throughout the whole frequency range R_s of Nb_3Sn is at least five times lower than R_s of niobium (always at 4.2 K). This advantage tends to improve towards higher frequencies because R_s^{BCS} increases with f^2 whereas R_{res} shows a weaker frequency dependence. The origin of parts of the residual resistance will be discussed in the next chapter.

Fig. 17 shows the reduced energy gap α obtained from our data.

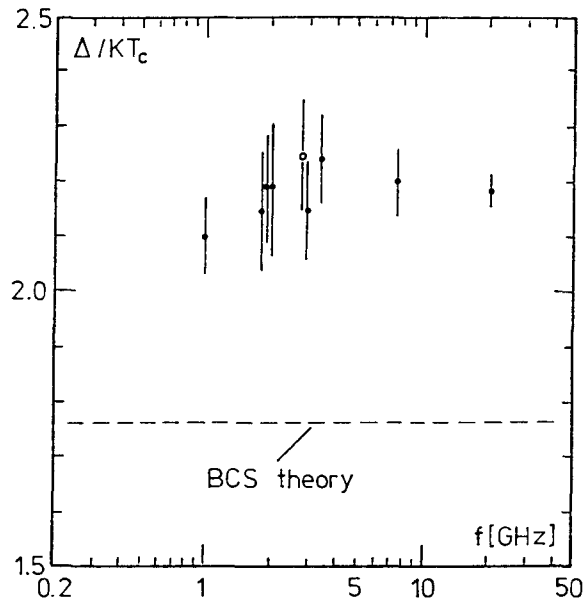

Fig. 17 :
Frequency dependence of the reduced energy gap $\alpha = \Delta/kT_c$ obtained from our data

There is no apparent frequency dependence of Δ/kT_c and its average value is 2.2±0.1 showing the strong coupling of the pairing interaction in Nb_3Sn.

5. ANOMALOUS LOSSES IN NB_3 SN CAVITIES

In our work during the last years special emphasis was devoted to the investigation of residual surface losses in Nb_3Sn cavities which are experimentally found to be higher than in niobium resonators.

5.1 Cool down dependent rf losses - evidence for thermoelectrically generated frozen in flux

A significant part of the residual losses in Nb_3Sn structures was found to be dependent on the cool down rate of the cavity.

Alternatively to the commonly used "fast cool down" to temperatures below T_c of Nb_3Sn by filling liquid helium into the cryostat, the cavity temperature was reduced very slowly (≅ 1 K/5 min) by a technique described in chapter 3.1. This method was applied on the 1 and 3 GHz single and multicell accelerating structures. In all cases the slow cool down resulted in a significantly increased cavity Q.
This effect is demonstrated in figures 18 and 19. There the cavity Q is plotted for a single and a five cell accelerator cavity as a function of the accelerating field E_a.

In the 3 GHz five cell cavity R_{res} was found to be independent of the temperature (no steps in R_{res} by indium or Nb-Sn phases different from Nb_3Sn turning superconducting) so that the theoretically expected cavity Q at 4.2 K could be determined by:

$$Q_{BCS}(4.2\ K) = (Q\ (4.2\ K)^{-1} - Q\ (2.2\ K)^{-1}\ ).$$

The result (Fig. 19) demonstrates that the strong Q (E) dependence is only due to R_{res}. The fact, that Q_{BCS} (4.2 K) = G/R_{BCS}(4.2 K) keeps constant also at comparibly high field levels indicates furthermore that the temperature increase of the inner cavity surface is negligible.

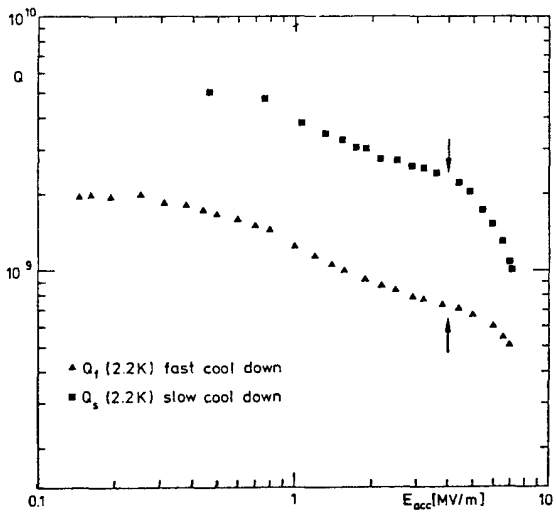

Fig. 18: Dependence of the cavity Q on the accelerating field after a fast cool down (lower curve) and after a slow cool down (upper curve). These curves were taken in a 3 GHz single cell cavity. Above E_{acc} = 4 MV/m (arrows) electron field emission loading was observed.

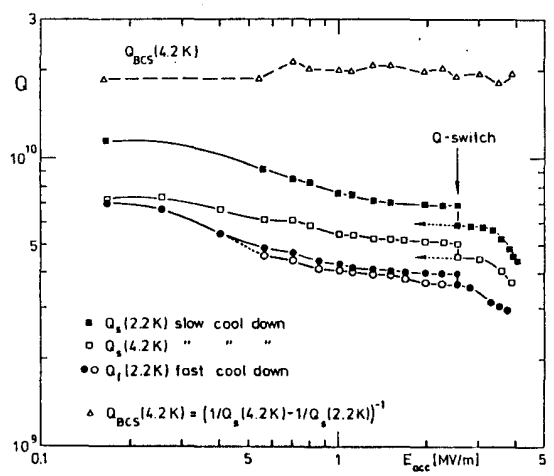

Fig. 19:
Cavity Q values of a five cell Nb_3Sn coated 3 GHz cavity as a function of accelerating field. The hysteresis in the curves results from a Q-switch which appeared at E_a = 2.6 MV/m and disappeared far below the switching field.

In Fig. 20 the spatial distribution of the rf losses taken in a 3 GHz single cell cavity after a slow (lower curve) and after a fast (upper curve) cool down is shown. It demonstrates that the additional losses are uniformly distributed over all the surface. The spikes in the heat flux density are caused by local defects. Their rf losses are independent of the cool down rate.

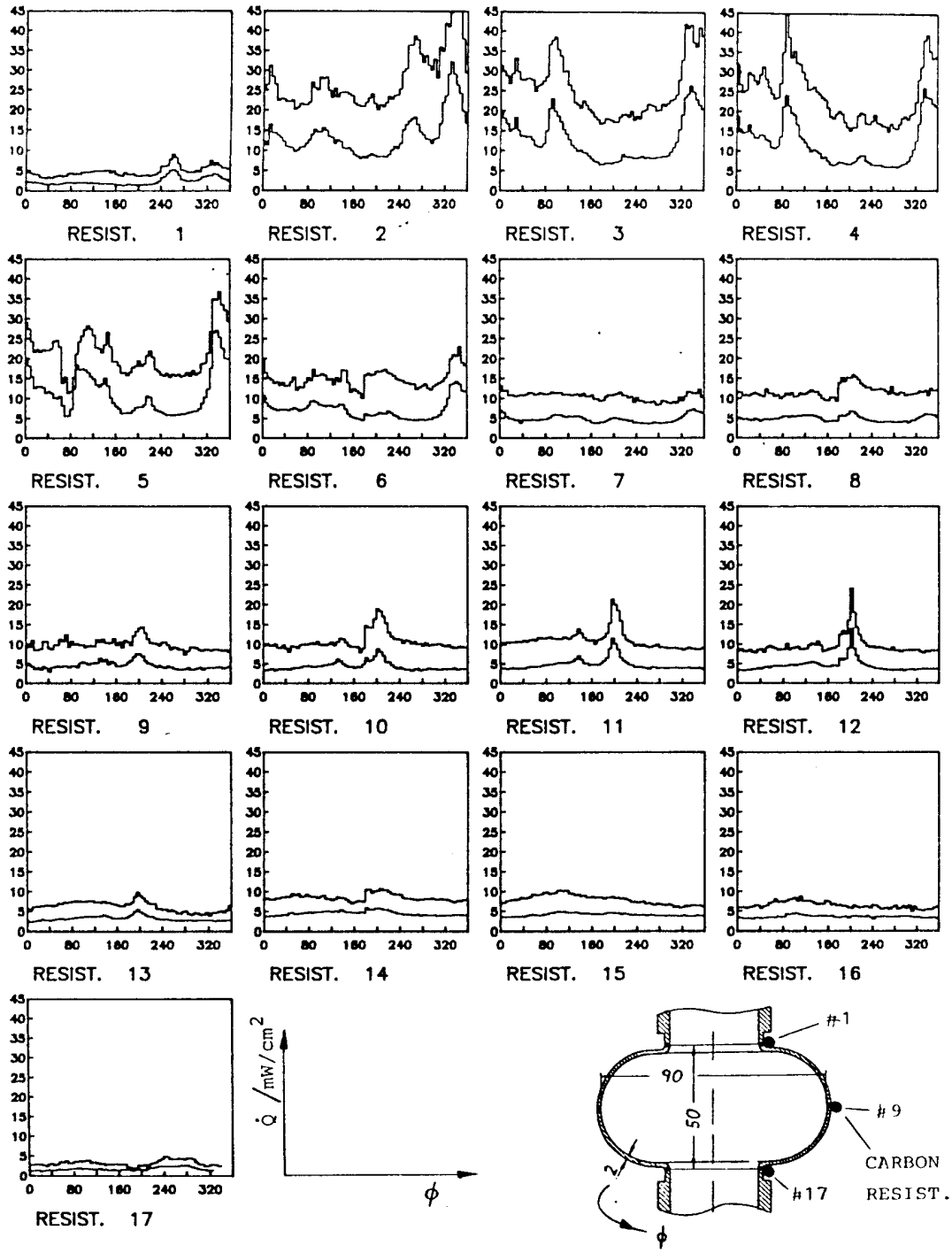

Fig. 20:
Spatial distribution of the rf losses in a 3 GHz single cell cavity after a slow cool down (lower curves) and after a fast cool down (upper curves). Both experiments are done at an accelerating field of 7 MV/m.

A further analysis of the cool down dependent losses in Fig. 20 indicates that these uniform losses after the fast cool down are not only higher than after the slow cool down but they also are within errors proportional to each other over all the cavity surface. From this observation one can conclude that even after the slow cool down the cavity Q is still limited by this cool down dependent mechanism.

Another effect was observed both in a 1 and 3 GHz single cell cavity. In Fig. 21 temperature maps taken in fundamental mode of the 1 GHz single cell cavity at E_a = 5 MV/m before and after a quenching of the cavity are shown. The spike at the "equator region" at an angle of 310° appears in both maps and gives the quench location after the initial quenching.

Beside this on both cups of the cell at about 200 ° local regions with enhanced rf losses occurred after the initial quenching and kept stable until the cavity was warmed up above the T_c of Nb_3Sn. After a further cool down these local regions of enhanced losses disappeared and the temperature map exhibited the same appearance as before the quenching. Similar effects were observed frequently after a thermal instability had caused a quenching of the cavity field.

These losses can also be connected to a rapid cool down process. During the local thermal instability a finite area of the rf surface and most likely also the underlying niobium wall increase their temperature well above 18.0 K. After the field is quenched by the high Joule losses in this normal conducting part of the cavity the quench area is cooled very rapidly below T_c.

Our present interpretation of the phenomena described in this paragraph is linked to thermoelectric currents. We assume that the thermovoltage between the niobium substrate and the Nb_sSn layer can lead to strong thermoelectric currents during the cooldown of a cavity when temperature gradients between different regions of the "Nb-Nb_3Sn sandwhich" develop. These currents may turn into persistent currents when both materials make their transitions to the superconducting state. This in turn leads to frozen in magnetic flux which generates normal conducting surface areas which then in turn are the origin of anomalous Joule losses. It should be possible to create such a mixed superconducting - normalconducting surface area on a Nb_3Sn sample cooled rapidly to 4.2 K and to make this mixed state visible by appropriate analytical procedures. Such experiments however have not yet been performed.

5.2. Nb_3Sn cavities cooled in an external magnetic field

From different experiments performed on superconducting cavities cooled down under an external magnetic field H_{ext} [29,30] it is well known that trapped magnetic flux causes an additional residual resistance R_H which may be parametrized by:

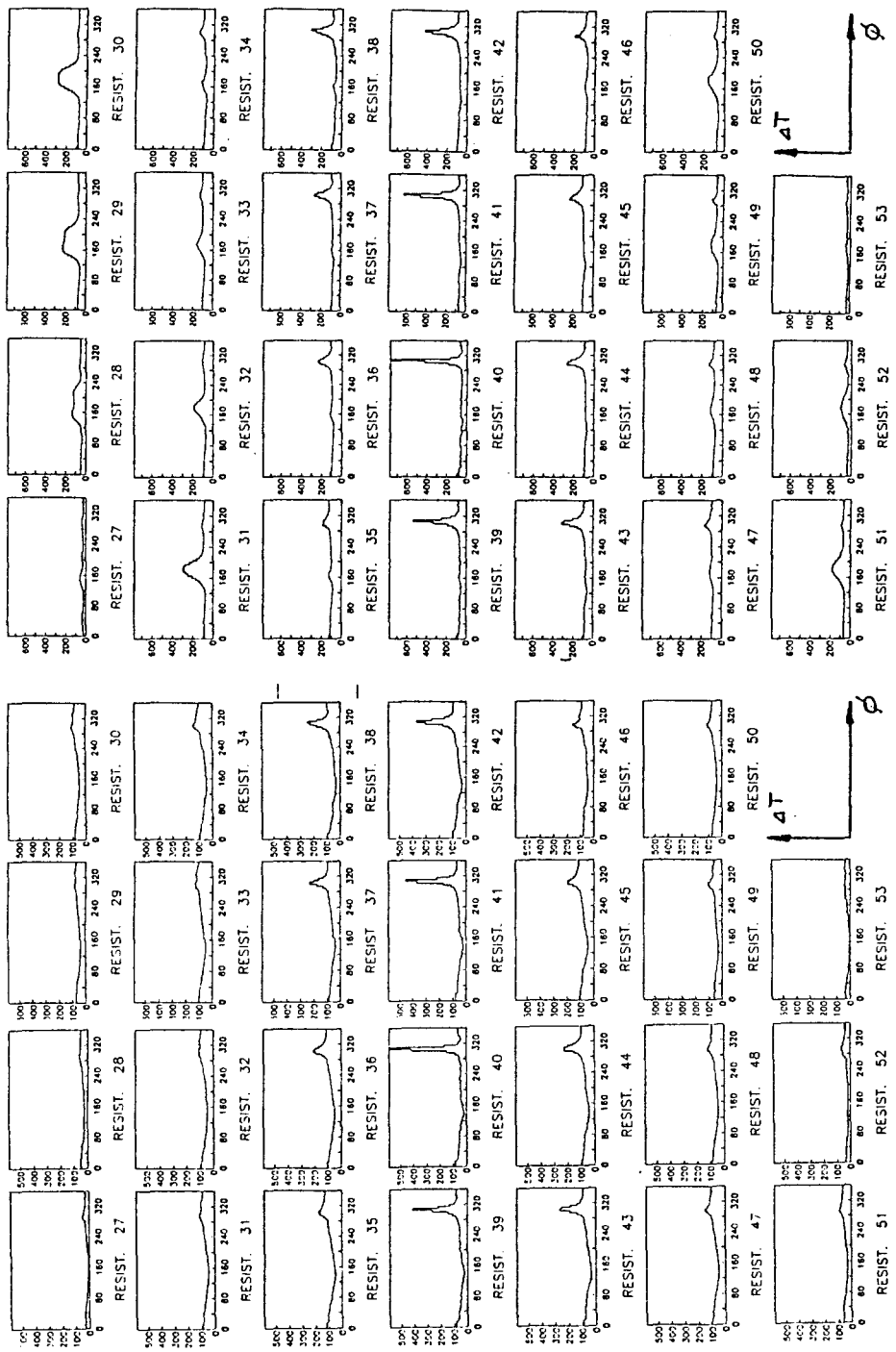

Fig. 21:
Temperature maps of a 1 GHz single cell cavity taken before (left) and after (right) a local thermal instability of the cavity. The accelerating field is 5 MV/m in both cases.

$$R = \gamma \cdot \frac{R_n \cdot H_{ext}}{Hc_2} \qquad (4)$$

where R_n represents the normal conducting surface resistance just above T_c and Hc_2 the upper critical field. The coefficient γ reflects the "effectivity" of the flux trapping and depends on the geometry of the sample. This relation takes into account the rf losses in the normal conducting cores of the fluxoids.

To further investigate residual losses originating from frozen in flux of external magnetic fields and to contribute to the understanding of the cool down dependent losses we performed single cell experiments at 3 and 21.5 GHz in external magnetic fields.

Fig. 22 shows Q (E_a) data of a 3 GHz single cell cavity cooled down in different external magnetic fields slow as well as fast. The increasing Joule losses with increasing external field are clearly seen.

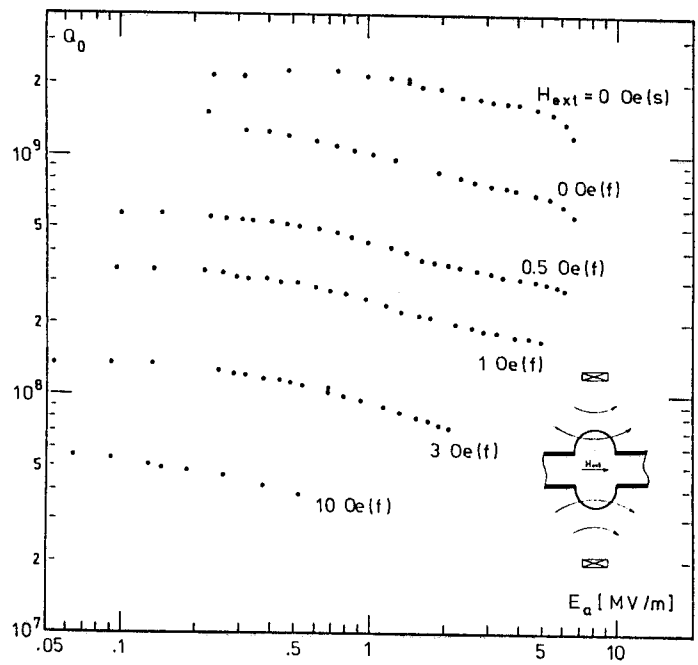

Fig. 22:
Cavity Q versus accelerating field curves taken in a 3 GHz single cell cavity after a slow cool down (s) and after fast cool down (f) in different external magnetic fields.

A similar experiment was performed with our K-Band cavity at 21.5 GHz. In Fig. 23 the residual resistance measured at very low rf fields in the cavities at 3 and 21.5 GHz is plotted as a function of the external magnetic field during cool down to the superconducting state. It is seen that the functional dependence on H_{ext} is found like given in equation (4).

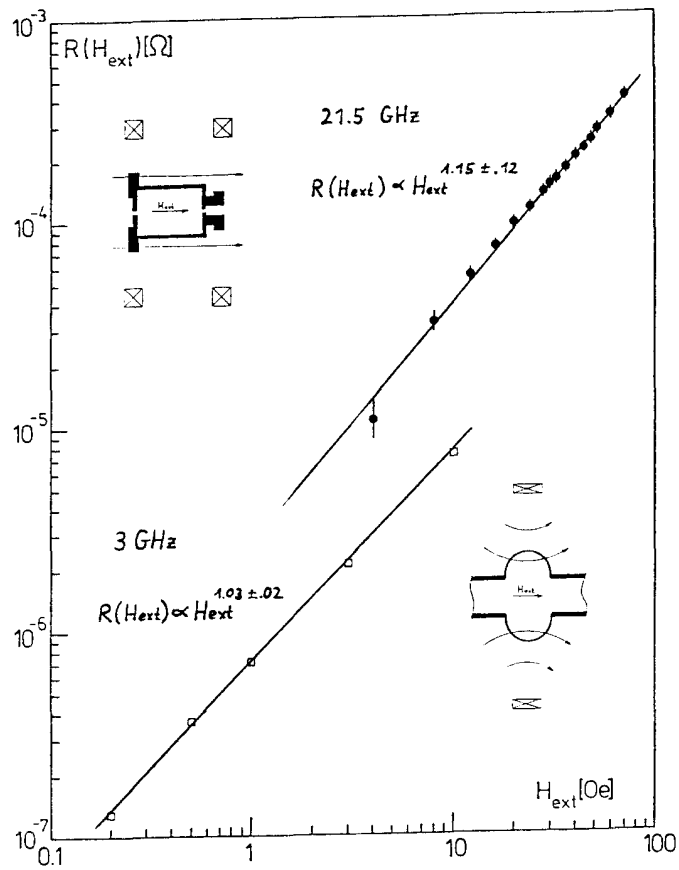

Fig. 23:
Surface resistance due to frozen in flux as a function of the external magnetic field applied during the cool down to the superconducting state. The data are taken for a 3 GHz single cell cavity (lower curve) and for a pill box cavity at 21.5 GHz.

A further analysis of these preliminary data is presently under progress.

5.3. Residual losses by "weak spots"

In Nb_3Sn cavities one can observe anomalous losses additional to those discussed in the proceeding chapters. Both in the L, S and K band resonators sudden increases in the rf losses at well defined fields ("Q switches") occur. In Fig. 24 temperature maps of the 3 GHz five cell cavity taken at fields below and above such Q switches are shown. It is clearly seen that small regions of the cavity surface switch to a high loss state at a given field. Fig. 19 documents that this additional loss mechanism is switched off at a field level far below the "switch on field". We assume that these Q switches are caused by small, maybe microscopic, weakly superconducting defects which switch from a superconducting to a normalconducting state. Since not significant temperature dependences of the switching fields are observed between 4.2 and 2 K we conclude that these weak s.c. spots have T_c values well above 4.2 K. Measurements at K band support this assumption [9,12].

A possible explanation is given by impurity inclusions in the niobium base material which disturb the uniform Nb_3Sn layer and which become weak superconductors by the proximity effect. Optical inspections of the rf surface at the location of the observed switch in most cases showed a defect in the Nb_3Sn layer at the same spot.

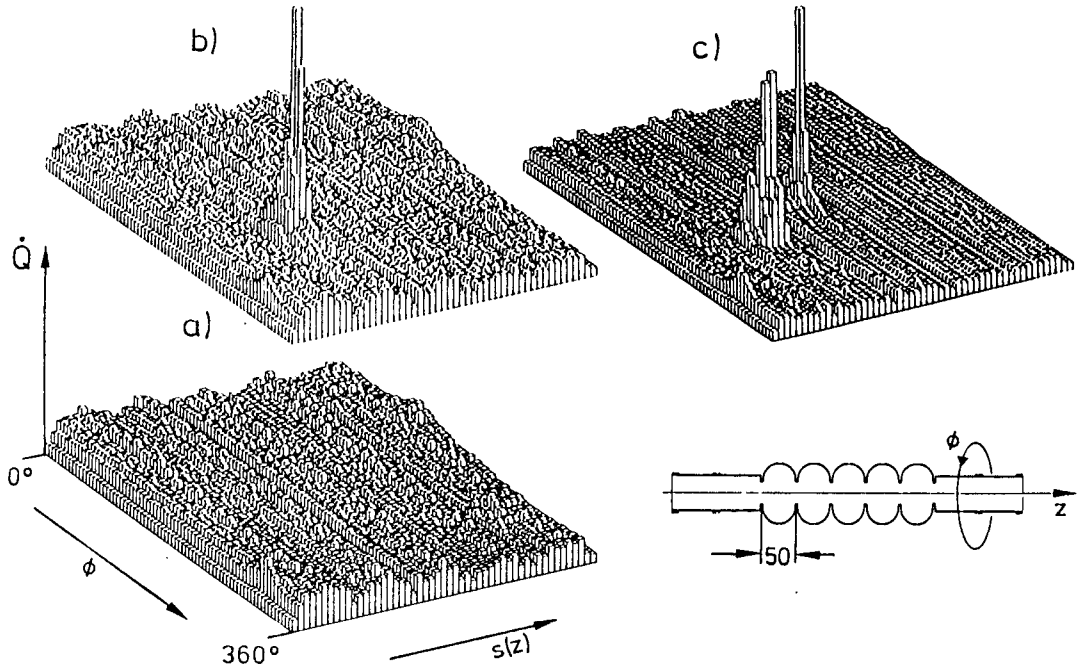

Fig. 24:
Spatial distribution of the rf losses in a 3 GHz Nb_3Sn coated five cell cavity taken at an accelerating field of 2.55 MV/m (a), 2.6 MV/m (b) and 3.9 MV/m (c). (Q in arbitrary units).

CONCLUSIONS

During the last three years it could be shown experimentally that Nb_3Sn covered accelerator cavities show considerably lower rf losses at 4.2 K than niobium cavities. At 1 GHz improvements of the losses by a factor of 10 at low field levels and about 4 at high field levels are readily obtained, an observation which becomes more favourable towards higher frequencies and reaches an improvement of 150 at 21.5 GHz. The accelerating fields of up to 7 MV/m obtained resemble very much the state of the art of niobium cavities of low purity by 1983. First experiments to deposit Nb_3Sn layers on high purity niobium have been unsuccessful but are continued with good expectations. Residual losses by frozen in magnetic flux created by thermoelectric currents during the cavity cool down or during quench events have been found to be a general phenomenon with superconducting Nb_3 Sn cavities. By proper procedures such losses can however be avoided. The next of our work in Wuppertal will be the preparation of Nb_3Sn cavities based upon the new high thermal conductivity niobium.

ACKNOWLEDGMENTS

We like to express our appreciation of our collaboration with DESY. Its technical and financial help was important for the accomplishment of our work. The contribution of J. Adam of the CERN SB-Division who very skillfully peformed the depth profile measurements of the Nb_3Sn samples is gratefully acknowledged.

We also thank H. Vogel for his support in calculating field distributions of the higher order modes in our cavities. The devoted work of R. Fleck during all of the 1 GHz experiments is highly appreciated.

This work was supported in part by the German Federal Ministery for Research and Technology (BMFT) under contract number O5 4WT 85I(1).

REFERENCES

1. G.Arnolds et al., IEEE Trans. MAG-15, No.1, 613,(1979).

2. B.Hillenbrand et al., IEEE Trans. MAG-13, No.1, 49(1977).

3. J.B.Stimmel, thesis, Cornell University (1978).

4. G.Arnolds, Doktorarbeit, University of Wupperrtal, WUB 79-14(1979).

5. G.Arnolds, H.Heinrichs, R.Mayer, N.Minatti, H.Piel, W.Weingarten, IEEE Trans. NS-26, 3775(1979).

6. R.Mayer, Doktorarbeit , University of Wuppertal, WUB 80-29 (1980).

7. M.Peiniger, Diplomarbeit, University of Wuppertal, WUD 83-1 (1983).

8. J.Ding, Diplomarbeit, University of Wuppertal, WUD 86-7 (1986).

9. N.Klein, Diplomarbeit, University of Wuppertal, WUD 85-5 (1985).

10. H.Diepers, B.Hillenbrand, H.Martens, O.Schmidt, K.Schnitzke, Y.Uzel, H.Wohlleben: Forschungsbericht BMFT-FB T74-19.

11. The SEM investigations on our Nb_3Sn samples were performed by J.Adams at CERN.

12. M.Hein, Diplomarbeit, University of Wuppertal, WUD 87-3 (1987).

13. D.Meschede, H.Walther, G.Müller, Phys.Rev.Lett. 54, 551 (1958).

14. G.N.Ronami et al., Izv. Akad.Nauk.SSSR Neorg.Mater. 7,1490(1971).

15. C.F. Old and I.Macphail, J.Mat.Science 4, 202(1969).

16. H.H.Farrell et al., Thin solid Film 25, 253(1975).

17. H.H.Farrell et al., J.Appl.Phys. 45, 4025(1974).

18. P.Kneisel et al., Adv.Cryog.Eng., Vol. 24, 442(1978).

19. G.Arnolds-Mayer and E.Chiaveri, CERN/EF/RF 86-2 (1986).

20. P.Thüns. Diplomarbeit, University of Wuppertal, WUD 87-16 (1987).

21. H.Padamsee in H.Lengeler, editor, Proc. of the Second Workshop on Rf-Superconductivity CERN, Geneva, 1984, p. 339.

22. H.Lengeler, W.Weingarten, G.Müller, H.Piel, IEEE Trans.MAG-21,1014 (1985).

23. R.Röth, Diplomarbeit, University of Wuppertal, WUD 86-16 (1986).

24. H.Piel and R.Romijn, CERN/EF/RF 80-3 (1980).

25. G.Müller, ibid ref. 21, p. 377.

26. D.Proch, Doktorarbeit, University of Wuppertal, WUB 78-11 (1978).

27. P.Kneisel et al., IEEE Trans. MAG-15, 21 (1979).

28. M.Peiniger, H.Piel, IEEE Trans NS-32, 3612 (1985).

29. B.Piosczyk et al., IEEE Trans NS-20,108 (1973).

30. B.Piosczyk, thesis, University of Karlsruhe (1974).

31. G.Rempe, H.Walther, N.Klein, Phys. Rev. Lett. 58, 353 (1987).